Experimental Eye Research 90 (2010) 277–284

Contents lists available at ScienceDirect

Experimental Eye Research

journal homepage: www.elsevier.com/locate/yexer

Dimensions of the human sclera: Thickness measurement and regional changes with axial length

Richard E. Norman [a,b], John G. Flanagan [c,d], Sophie M.K. Rausch [a,e], Ian A. Sigal [f], Inka Tertinegg [c], Armin Eilaghi [a,b], Sharon Portnoy [g], John G. Sled [g], C. Ross Ethier [a,b,c,h,*]

[a] Mechanical and Industrial Engineering, University of Toronto, Toronto, Ontario, Canada
[b] Institute of Biomaterials and Biomedical Engineering, University of Toronto, Toronto, Ontario, Canada
[c] Ophthalmology and Vision Sciences, University of Toronto, Toronto, Ontario, Canada
[d] School of Optometry, University of Waterloo, Waterloo, Ontario, Canada
[e] Institute for Computational Mechanics, Technische Universität München, Munich, Germany
[f] Ocular Biomechanics Laboratory, Devers Eye Institute, Portland, Oregon, USA
[g] Medical Biophysics, University of Toronto, Toronto, Ontario, Canada
[h] Department of Bioengineering, Imperial College London, London, United Kingdom

ARTICLE INFO

Article history:
Received 26 May 2009
Accepted in revised form 2 November 2009
Available online 11 November 2009

Keywords:
sclera
glaucoma
biomechanics
optic nerve head
lamina cribrosa
drug delivery

ABSTRACT

Scleral thickness, especially near the region of the optic nerve head (ONH), is a potential factor of interest in the development of glaucomatous optic neuropathy. Our goal was to characterize the scleral thickness distribution and other geometric features of human eyes. Eleven enucleated human globes (7 normal and 4 ostensibly glaucomatous) were imaged using high-field microMRI, providing 80 μm isotropic resolution over the whole eye. The MRI scans were segmented to produce 3-D corneoscleral shells. Each shell was divided into 15 slices along the anterior–posterior axis of the eye, and each slice was further subdivided into the anatomical quadrants. Average thickness was measured in each region, producing 60 thickness measurements per eye. Hierarchical clustering was used to identify trends in the thickness distribution, and scleral geometric features were correlated with globe axial length. Thickness over the whole sclera was 670 ± 80 μm (mean ± SD; range: 564 μm–832 μm) over the 11 eyes. Maximum thickness occurred at the posterior pole of the eye, with mean thickness of 996 ± 181 μm. Thickness decreased to a minimum at the equator, where a mean thickness of 491 ± 91 μm was measured. Eyes with a reported history of glaucoma were found to have longer axial length, smaller ONH canal dimensions and thinner posterior sclera. Several geometrical parameters of the eye, including posterior scleral thickness, axial length, and ONH canal diameter, appear linked. Significant intra-individual and inter-individual variation in scleral thickness was evident. This may be indicative of inter-individual differences in ocular biomechanics.

1. Introduction

The dimensions of the sclera are of physiological interest. In addition to being important for planning ophthalmic surgery and for the development of transscleral drug delivery (Lee et al., 2004; Olsen et al., 1998), they play a role in determining the biomechanical environment within the eye. In particular, because the sclera is the principal load-bearing tissue of the eye, differences in scleral properties can greatly affect the eye's mechanical strength—and hence its biomechanical response to intraocular pressure (IOP) (Sigal et al., 2005, 2009b). This is of particular interest in understanding the role of IOP in the pathogenesis of glaucomatous optic neuropathy, since scleral deformations due to IOP are transmitted to the tissues of the ONH, including the lamina cribrosa. These deformations create stresses and strains in ONH tissues which have been hypothesized to play a role in retinal ganglion cell loss in glaucoma (Burgoyne et al., 2005; Quigley et al., 1980).

The main features of the sclera that determine the biomechanical environment of the ONH tissues are the material properties of the sclera (effective stiffness) and the anatomical features of the sclera (thickness and globe size) (Sigal et al., 2005, 2009a). Human scleral thickness has been investigated previously using a variety of approaches, each with significant limitations. Several studies have used ultrasound biomicroscopy, which has the

* Corresponding author at: Department of Bioengineering, Imperial College, Exhibition Road, South Kensington Campus, London SW7 2AZ, United Kingdom. Tel.: +44 (0) 20 7594 9795; fax: +44 (0) 20 7594 9787.
E-mail address: r.ethier@imperial.ac.uk (C.R. Ethier).

0014-4835/$ – see front matter © 2009 Elsevier Ltd. All rights reserved.
doi:10.1016/j.exer.2009.11.001

advantage of allowing in vivo measurement, but is typically only able to measure scleral thickness up to approximately 3.0 mm posterior to the scleral spur (Lam et al., 2005; Oliveira et al., 2006). The scleral thickness in the vicinity of the optic nerve head (ONH) at the posterior of the eye — which is of particular interest in glaucoma — cannot be resolved with this technique. Lam et al. (2005) attempted to use MRI of patients to measure scleral thickness, but found that unavoidable random eye movements blurred the images leading to reduced accuracy. Olsen et al. (1998) hemisected donor eyes and then photographed their silhouettes against a scale. This provided scleral thickness measurements, but they were restricted to the single cutting plane used in the hemisection. Because there can be significant variations in scleral thickness within a single eye, and because the biomechanical environment in the ONH likely depends on the response of the entire sclera, it is beneficial to understand scleral thickness distributions across the entire globe.

The goal of this study was to more completely characterize the scleral thickness distribution of human eyes. For this purpose we used high-field microMRI measurements of whole post-mortem eyes. We also investigated the relationship between scleral thickness, axial length and ONH canal diameter.

2. Materials and methods

Eleven enucleated human donor eyes (five pairs and a single additional eye) were obtained from the Eye Bank of Canada within 24 h of death. Seven of these eyes were identified as normal, while four were reported to the Eye Bank as being glaucomatous by family members. The age of the donors ranged between 70 and 83 years. In the case of the eyes identified as ostensibly glaucomatous, the nature of the disease (i.e. whether it was simply ocular hypertension or symptomatic glaucoma) was not available. Multiple attempts were made to gain access to more detailed medical records for all eyes, but logistical and confidentiality issues precluded this.

In an attempt to confirm the diseased status of the eyes, all eyes were imaged by scanning laser tomography imaging (Heidelberg Retina Tomograph; HRT) and had their optic nerves assessed. Imaging was performed using a methodology described previously (Sigal et al., 2004). In terms of chronological sequence, the eyes were imaged after the fixation and MR imaging process described below. Cup to disc ratios (C:D ratio) were calculated manually from inspection of the images by an observer who was unaware of the identity of the eyes. Three of the four ostensibly glaucomatous eyes had optic nerve head appearances that were consistent with a diagnosis of glaucoma, that is they had large vertical cup to disc ratios (C:D ratio), relative narrowing of the superior and inferior neural rim tissue (did not obey the ISNT rule (Fingeret et al., 2005)), and/or localised thinning (notching) of the superior or inferior neural rim tissue. The remaining ostensibly glaucomatous eye, despite being one of pair, had a more normal looking neural rim appearance. Three of the "normal" eyes had large cups (vertical cup:disc ratio > 0.6). It should be noted that HRT analysis alone is not sufficient to confirm glaucoma and would usually be combined with other clinical data (e.g. optic disc photos and perimetry) when making a clinical diagnosis. These latter tests cannot be performed on post-mortem eyes, however. Because of the novel measurement approach used in this work, the difficulty of acquiring donor tissue, and the potential for rare insight into glaucoma it was decided to include the ostensibly glaucomatous eyes in the study despite being unable to definitively confirm their status with supplemental techniques.

Prior to MR imaging, the eyes were fixed with 10% formalin in phosphate buffered saline (PBS) for 24 h at either 5 mmHg (OD; $n = 5$) or 50 mmHg (OS; $n = 6$). The IOP was set by cannulating the eyes and then attaching each eye individually to a reservoir containing 10% formalin in PBS raised to a calibrated height. The large range in IOP was chosen in order to ensure that any effects on globe size or other structural factors, if present, would be measurable; the scarcity of donor tissue precluded experimenting with different fixation pressures. After fixation, the eyes were bathed for 4 days in PBS and then for 12 days in PBS containing 2 mM gadoteridol (ProHance, Bracco Diagnostics, Inc., Princeton, NJ), an MRI contrast agent used to improve imaging quality. The eyes were then dipped in 3% agar in 2 mM gadoteridol until the coating reached approximately 2 mm in thickness. They were then placed in 50 ml tubes. To prevent the eyes from shifting during the scan, the tubes were filled with glass beads. Fluorinert FC-77 (3M Company, St. Paul, MN) was then poured into the tube to fill the remaining space between beads. Fluorinert was chosen because it allowed for the tissue to be suspended while avoiding the unwanted MR signal that would come with immersion in water; furthermore, it is immiscible in water and, in our experience, does not infiltrate tissue, preventing potential scan distortion or effects on tissue. The combination of agar and glass beads with Fluorinert created a high contrast boundary at the outer edge of the sclera, making later identification of the anatomical boundaries straightforward. The eyes were scanned using a 7.0 T MRI scanner (Varian, Inc., Palo Alto, CA). MR images were acquired using a three dimensional spin-echo pulse sequence with the following parameters: 325 ms repetition time (TR), 10 ms echo time (TE), 4 cm $\times$ 3 cm $\times$ 3 cm field of view (FOV), and 80 micron isotropic resolution.

The corneoscleral shells of the eyes were manually segmented using Amira 3.11 software (Mercury Computer Systems, Inc., Chelmsford, MA). Segmentation was performed with the aid of a tablet as outlined in Fig. 1. Only the corneoscleral shell was segmented, as it was the focus of this work. All eyes were segmented by a single observer who was unaware of the identity of the eye. The segmentation was then reviewed in all three planes of the scan by two other observers to ensure consistent tissue identification. Segmenting in all three planes of the image helped to minimize the effects of obliqueness of the sections, which might lead to incorrect identification of anatomical boundaries and a distorted segmentation. A segmentation was "passed" when consensus was reached on the location of landmarks, delineations between tissues, and other features. Because of the workload involved in segmenting an individual eye by hand (approximately 1200 images in total, each of approximately 400 by 400 pixel resolution, demanding more than a week of full-time labour), it was not feasible to have multiple segmentations of whole eyes performed for a repeatability analysis. Next, Amira was used to generate corresponding surface meshes using a generalized marching cubes algorithm. Sub-voxel interpolation was used during this process to increase the smoothness of the mesh, but this still resulted in an aliased surface. To eliminate this aliasing and reduce the computational demands of the surfaces, the surfaces were simplified and smoothed to approximately 600,000 elements in Amira (Norman, 2008). Measurements of thickness and volume before and after the smoothing process revealed no significant changes in either quantity.

The corneoscleral shells were oriented along the anatomical planes (i.e. inferior-superior and temporal-nasal) based on the position of the extraocular muscles, the location of the macula relative to the ONH on the MRI scans, and examination of the actual eyes. The anterior–posterior axis was aligned to pass through the center of the ONH and the center of the cornea; although this is not the visual axis of the eye, it leads to more information about scleral thickness relative to the ONH. This approach was chosen because the underlying motivation of this work was the investigation of glaucomatous optic neuropathy, in which the ONH is a region of particular interest. Information regarding thickness relative to the ONH is

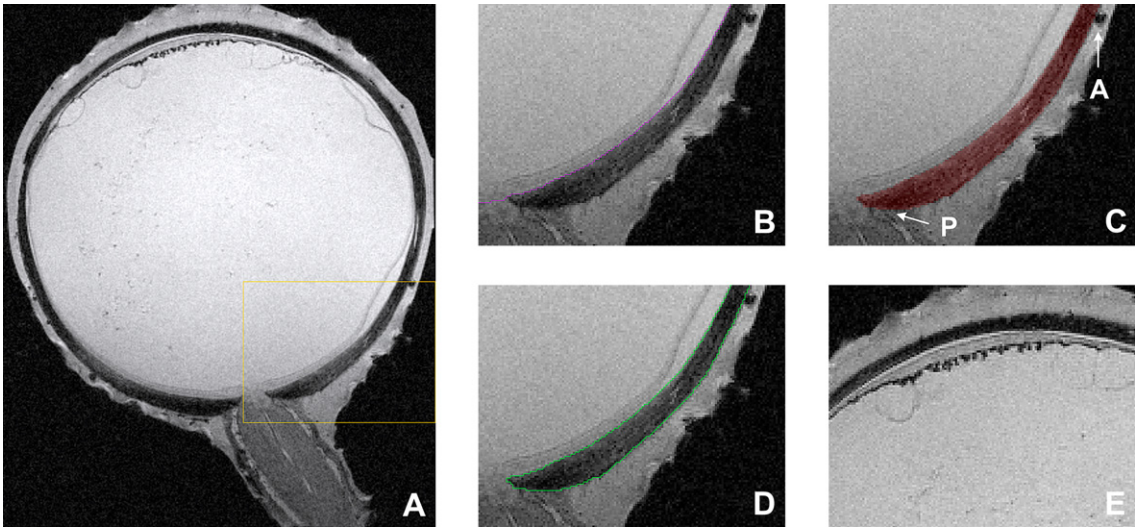

Fig. 1. Segmentation process for an image. Panel A shows a representative image of a human eye imaged at 80 μm isotropic resolution by microMRI. The dark sclera is clearly distinguished from the lighter interior of the eye and the agar coat on the exterior of the eye. Note that details such as the lumen of a central retinal vessel and the cupped shape of the ONH are apparent. The segmentation process began with semi-automated region-growing and threshold-based segmentation (Amira's "Magic Wand" and "Blow" tools, respectively) to separate the bright interior of the eye, choroid, and retina from the inner face of the sclera (purple line in panel B). This line was then used as a guide during the segmentation of the sclera, which was painted manually using a computer tablet. Painting was done using a transparent mask at increased magnification (panel C and yellow square in panel A), allowing for visualization of small features. This was of particular importance when identifying landmarks (e.g. the intersection of the sclera and the pia mater, arrow P, in panel C) and when identifying discrepancies in the image (e.g. a bubble in the agar at arrow A). In the case of discrepancies, the isotropic nature of MRI was particularly useful: a discrepancy that is not apparent in a particular image may be obvious in a neighbouring image, or in an alternative orientation. This compares favourably to histology, which is prone to alignment errors between slices and is not isotropic (as inter-slice resolution is typically below the resolution of a single image). The final segmentation generated for the region shown in panels B and C is shown in panel D. Once segmented completely in a first plane, each eye was then reviewed along the two remaining planes. This was often useful when the poor orientation of a given structure gave an equivocal interpretation. Panel E shows an oblique cross-sectional view of the ciliary processes. Regions such as this, which run directly alongside the sclera, proved problematic during initial experiments with automated segmentation. It was found that current algorithms, which typically work by separating regions of different intensity, incorrectly grouped the sclera with other adjacent dark structures. The extensive manual review necessary to correct these mistakes ultimately meant that it was both faster and less error-prone to adopt a manual segmentation process.

also useful for constructing more physiologically accurate computer models of this region.

Thickness measurement of the sclera was performed in Amira using its internal tool. In total, approximately 150,000 distances were calculated over the whole corneoscleral shell. Tests of this method on geometry of known dimensions revealed measurement errors of less than 1%.

Post-processing of the thickness data was performed using MATLAB (The Mathworks, Inc., Natick, MA). The eyes were divided into 15 equal-length radial slices along the anterior–posterior axis of the eye; the length of the slices scaled relative to the axial length of the eye. Each of these 15 circumferential slices was then divided into four quadrants: inferior, superior, nasal, and temporal. This produced a total of 60 regions across the entire surface of the corneoscleral shell, as illustrated in Fig. 2. Mean thicknesses were calculated for each region by analyzing the corresponding data points from the whole shell measurements, producing 60 measurements to characterize the thickness of the whole corneoscleral shell. The limbus occurred at slice 12, and all scleral thickness statistics were based on slices 1–12, i.e. excluding the cornea.

The axial length was measured in MATLAB from the most posterior aspect of the corneoscleral shell to the most anterior aspect of the cornea along the anterior–posterior axis (as illustrated in panel (B) of Fig. 2) using geometry data from the 3-D corneoscleral shells. This means that the axial lengths reported in this study are slightly larger than those measured clinically, as the latter measurements would typically measure only from the cornea to the surface of the internal limiting membrane. The optic nerve canal diameter was also measured in MATLAB using an averaging approach. In this method, the ONH canal was aligned on an axis passing through its center. Radial distances from the axis to the canal wall were calculated along the entire length and circumference of the ONH canal. These distances were then averaged to produce an average canal diameter for the entire canal. This is a different approach than used previously (cf. Jonas et al. (1988)) largely made possible by the 3-D nature of the dataset. Scleral volume was calculated by summing the volume of the individual elements comprising the 3-D corneoscleral shells in Amira.

Statistically related regions of thickness in the eye were identified via hierarchical clustering analysis using a Euclidean distance metric and single linkage in MATLAB. This analysis is used to reveal similarities between datasets composed of multiple measurements. It does this by comparing how similar the values composing separate factors are; in our case, the factor of interest was scleral thickness in each radial slice. If all of the corresponding values of two factors are similar to one another, the distance calculated between them will be small. This can be interpreted as meaning that the two factors are correlated or related. If the values are disjoint between two factors, a large distance will be calculated, and it can be concluded that the two factors being measured are likely unrelated. An agglomerative model can be used to build a tree of relationships based on the distance measurements: groups with short distances between them will be located close to each other on the tree. This representation can be useful for identifying ways to group data. Student's t test was used to identify statistical differences between populations. Pearson's correlation coefficient was used to test for linear relationships.

Some of the eyes considered in this work were from pairs, and it can reasonably be expected that parameters measured from fellow eyes are not statistically independent from one another. Because of the small sample size of this study and the ensuing limited gains in statistical power, an interactive correlation approach such as that suggested by Rosner (1982) was not used to compensate for the

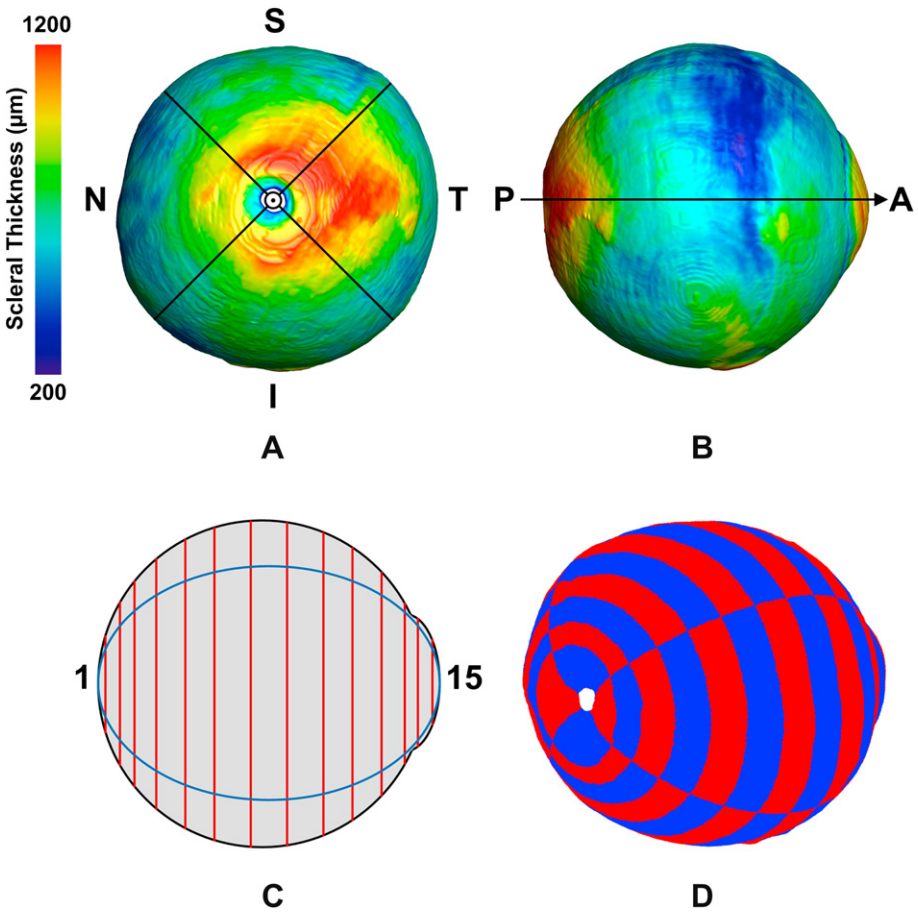

Fig. 2. (A) and (B) show posterior and temporal views of a 3-D corneoscleral shell with the measured thickness contours superimposed. Thickness was measured at approximately 150,000 points per eye. The anatomical axes are illustrated: nasal (N), temporal (T), superior (S), inferior (I), posterior (P), and anterior (A). The orientation of the anterior–posterior axis through the ONH and cornea is shown. The regions used to measure the mean regional and circumferential thicknesses of the eye are shown in diagram (C). Fifteen circumferential slices (red), numbered sequentially from the posterior pole (1) to the cornea (15), were made along the anterior–posterior axis. These circumferential slices were further subdivided into the four quadrants (blue) for some measurements. The region division of a corneoscleral shell from a posterior-temporal perspective is shown in (D). The thicknesses measured at all points contained in a region were averaged to produce the mean regional measurements used in later analysis.

inherent statistical similarities of paired eyes during statistical testing. Instead, in the case of paired eyes, a single eye was chosen at random for inclusion in statistical tests. Specifically, three OS and three OD (corresponding to three low pressure and three high pressure eyes) were selected in total, two of which were ostensibly glaucomatous.

3. Results

The average thickness of the whole scleral shell across all eyes was 670 ± 80 μm (mean ± SD; $n = 11$), with a range of 564 μm to 832 μm. Fig. 3 shows the mean scleral thickness and standard deviation from the posterior of the eye to the corneoscleral limbus for the four anatomical quadrants of the eye and a circumferential average. Significant intra-individual variation in scleral thickness was observed: the average ratio between the mean thickness of the thickest and thinnest region of sclera on an eye was 3:1. The thickest region of sclera was observed at the posterior pole of the eye, averaging 996 ± 181 μm across the eyes. The thinnest sclera occurred at the equator, measuring 491 ± 91 μm. Scleral thickness near the corneoscleral limbus was 588 ± 63 μm. A trend of thickening of the inferior quadrant was observed at the equator.

Hierarchical clustering was performed on the circumferential average thickness distribution (i.e. all four quadrants measured together) in order to identify trends in the regional distribution of scleral thickness across the eyes. Three regions of thickness were identified in the sclera: posterior polar, posterior-equatorial, and equatorial. The remainder of the corneoscleral shell is made up of the cornea. These radial regions correspond to 0–10%, 10–25%, 25–90%, and 90–100% of the eye's axial length measured from the ONH, respectively. Fig. 4 shows a contour plot of the circumferential thickness distributions of the 11 eyes with the three regions identified.

Correlations were observed between axial length and canal diameter ($r = -0.966$, $p = 0.02$) and axial length and thickness of the first scleral slice adjacent to the ONH ($r = -0.751$, $p = 0.085$) across the subset of eyes statistically analyzed. Scatter plots of the data support these observations (Fig. 5). To investigate whether scleral thinning was associated with changes in the distribution of scleral tissue over the eye, the posterior scleral volume (comprising the five circumferential slices of the posterior polar and posterior-equatorial thickness regions) was measured. This region was defined based on the results of the hierarchical analysis, which suggested that the posterior-equatorial region marked where the characteristic scleral thickening associated with the ONH began. A ratio of this volume to total scleral volume was calculated, indicating the relative amount of total scleral volume located at the posterior of the eye. A correlation coefficient of −0.479 was calculated between axial length and this quantity, but the correlation was found not to be significant ($p = 0.17$).

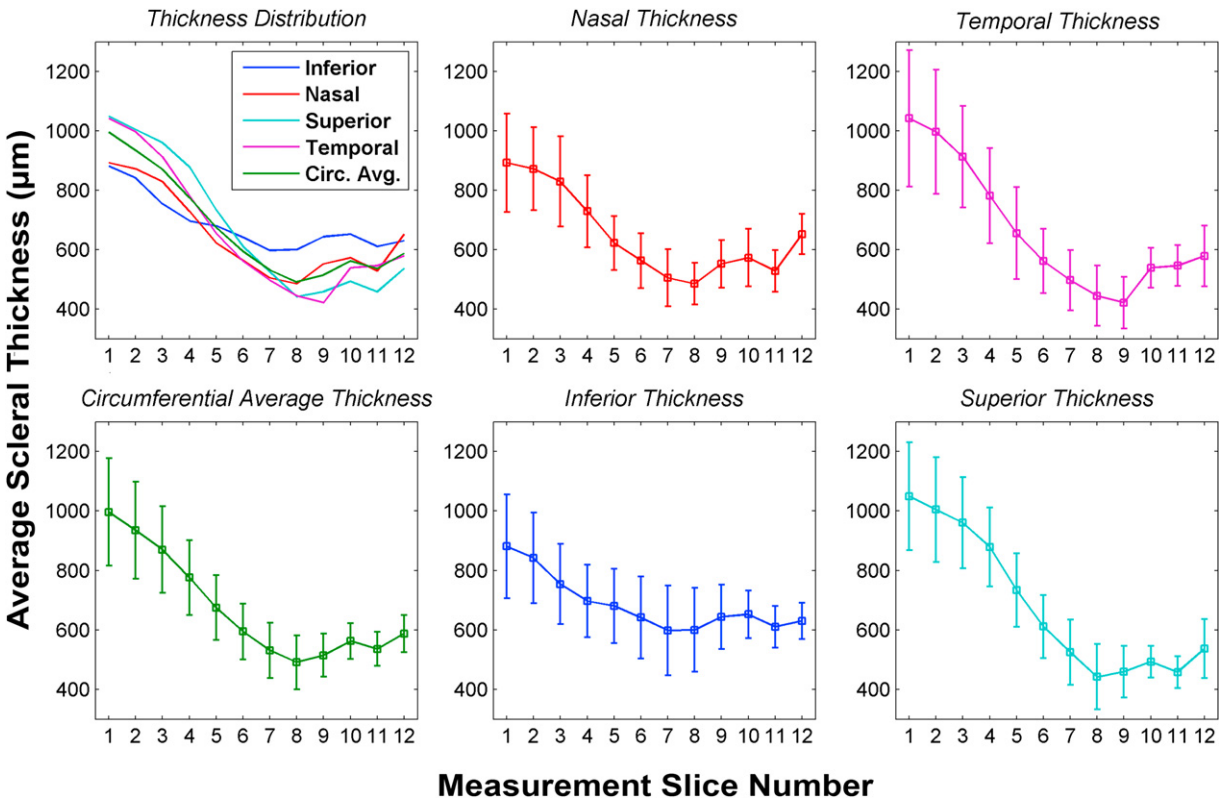

Fig. 3. Average scleral thickness distribution of 11 human eyes. A comparison plot of the regional measurements is shown in the top left. The scleral thickness distribution ± standard deviation of each of the four anatomical quadrants is plotted as well as a circumferential average including all four regions together. The slices are numbered sequentially from the posterior of the eye (left) to the limbus (right).

The axial lengths, mean scleral thickness, and thickness of the sclera adjacent to the ONH were compared in the low- and high-pressure fixation groups to determine whether scleral thinning could be mechanically induced by differences in IOP. No significant difference was found between the groups (comprising all 11 eyes in the study) for all three measures ($p = 0.85$, $p = 0.42$, and $p = 0.24$, respectively).

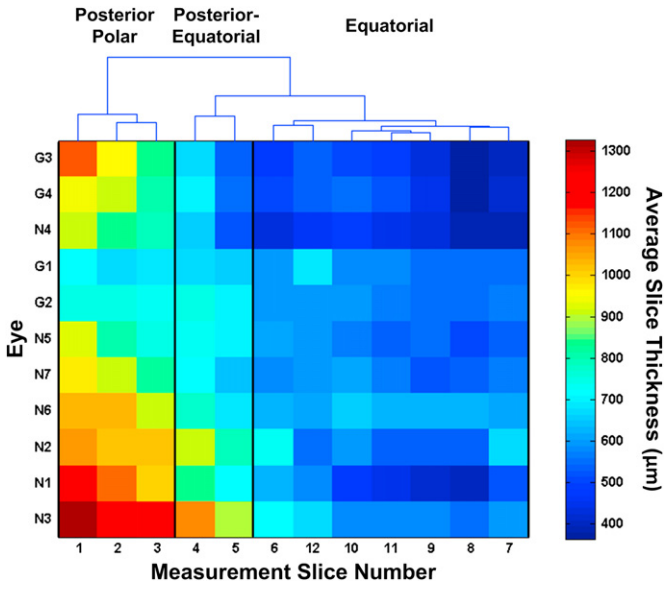

Fig. 4. Three thickness regions of the human sclera as identified by hierarchical clustering. For example, the posterior polar region consist of slices 1, 2, and 3. The measurement slice results and eyes have been ordered to best illustrate the regions. Each row represents the circumferential thickness distribution of one eye. A dendrogram representing the hierarchical clustering results is shown at the top of the figure. Normal (N) and ostensibly glaucomatous (G) eyes are identified.

Because of the small sample size of the study, the ostensibly glaucomatous eyes were included with the normal eyes when calculating the thickness distribution. Some trends were observed in these eyes, however, that may be of interest in light of their ostensibly glaucomatous status. The ostensibly glaucomatous eyes tended to be axially-elongated, had smaller ONH canal diameters, and had thinner posterior sclera. The mean axial length was 27.2 ± 0.7 mm (mean ± SD) for the ostensibly glaucomatous and 25.2 ± 0.5 mm for normal eyes. The average ONH canal diameter of the ostensibly glaucomatous eyes was 2.03 ± 0.16 mm versus 3.09 ± 0.44 mm in normal eyes. The vast majority of the narrowing in the ostensibly glaucomatous eyes occurred at the posterior end of the ONH canal. The mean anterior canal diameter, which corresponds to the region associated with the optic disc, was found to be similar between the two groups: it measured 1.87 ± 0.36 mm versus 1.95 ± 0.73 mm in normal eyes.

Fig. 6 shows the average circumferential thickness distribution for the pooled eyes, as well as distributions for the normal and ostensibly glaucomatous subgroups. A trend of thinning at the posterior pole of the eye in the ostensibly glaucomatous subgroup is apparent, although this effect was not significant. The average equatorial thickness of both normal and ostensibly glaucomatous eyes is comparatively similar, suggesting that if scleral thinning is present, it may occur preferentially at the posterior of the eye.

The C:D ratio for the eyes was compared against scleral thickness adjacent to the ONH and the posterior scleral volume. A significant linear correlation was observed between C:D ratio and posterior scleral volume ($r = -0.818$, $p = 0.05$). This is illustrated in Fig. 7.

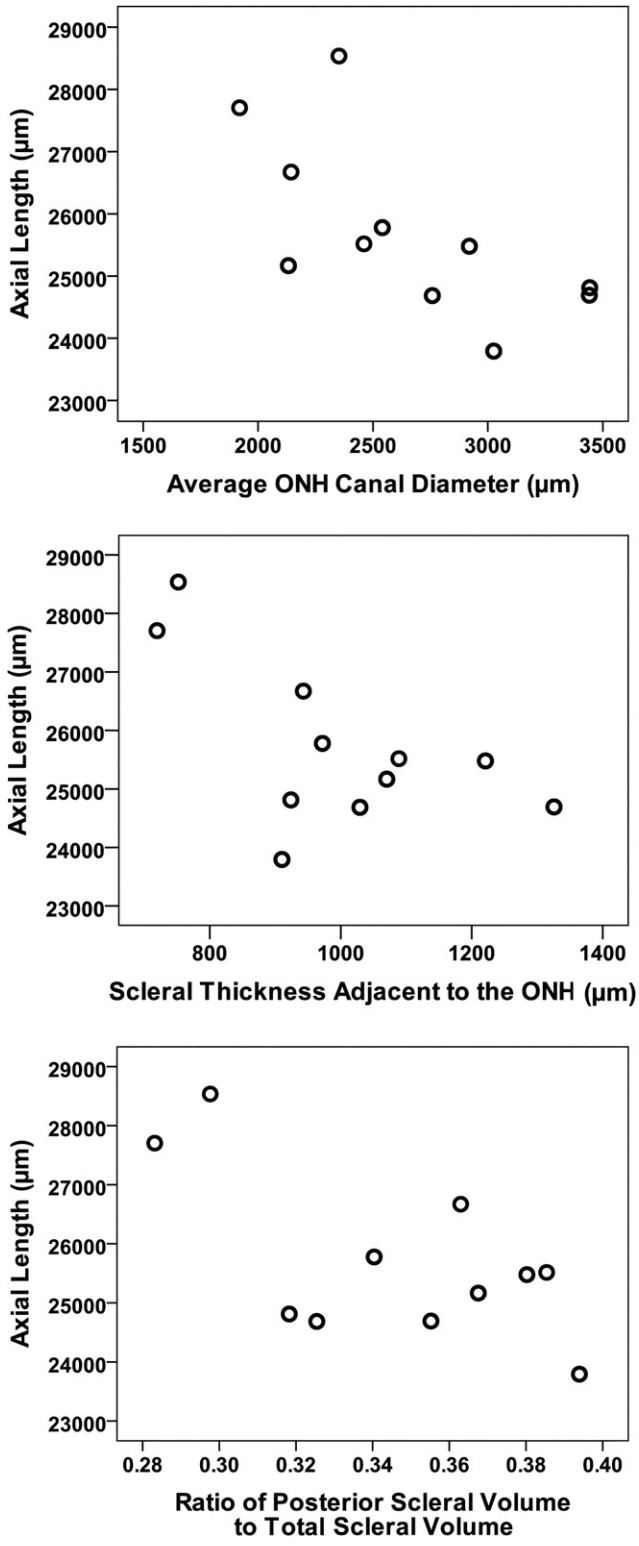

Fig. 5. Scatter plots of axial length and ONH canal diameter, axial length and posterior scleral thickness, and axial length and the ratio of posterior volume to total scleral volume. Each point represents one eye.

4. Discussion

The goal of this study was to characterize the scleral thickness distribution of the human eye in order to better understand its possible role in the pathogenesis of glaucoma. The significant

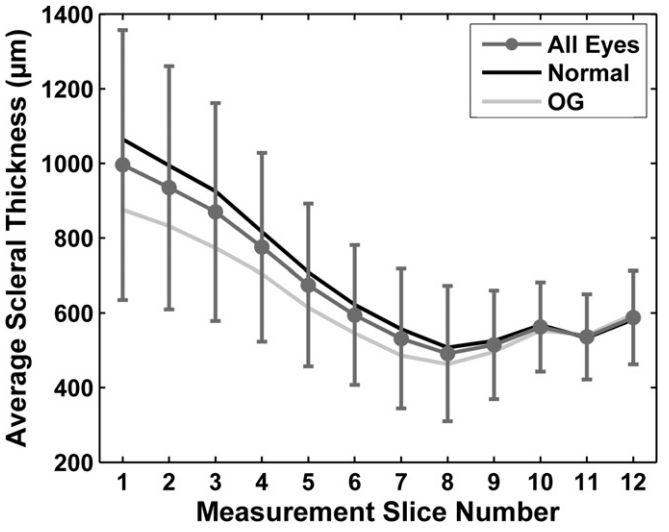

Fig. 6. Average circumferential thickness distribution for all eyes (mean ± standard deviation) compared to mean distributions for the normal and ostensibly glaucomatous (OG) subgroups. Ostensibly glaucomatous eyes may have thinner sclera relative to normal eyes. An expanded study is necessary to confirm this finding due to the large inter-individual variability evident in the data. The equatorial thicknesses (corresponding to slices 6 through 12) appear comparatively similar between the two subgroups, suggesting that thinning, if present, may occur preferentially in the posterior region of the eye.

variability in scleral thickness observed between individuals may be important, as this likely has great effects on the mechanical behaviour of the eye. Differences in the way that the eye responds to IOP may predispose some eyes to IOP-induced damage.

This study is consistent with the results of other human scleral thickness studies, as our thickness distribution corresponds well to that observed by Olsen et al. (1998). Our equatorial and corneoscleral limbus measurements are higher (they report 0.39 ± 0.17 mm and 0.53 ± 0.14 mm), but this can be explained by our inclusion of measurements from the entire circumference of the eye rather than just a single plane. Olsen's cut traversed only the nasal–temporal plane of the eye, which our measurements show to have thinner sclera on average. Large intra-individual variability in scleral thickness was observed in both this study and Olsen's, which may have significant biomechanical implications.

The correlation between axial length and thinning of the posterior region of the sclera is consistent with studies by Guthoff

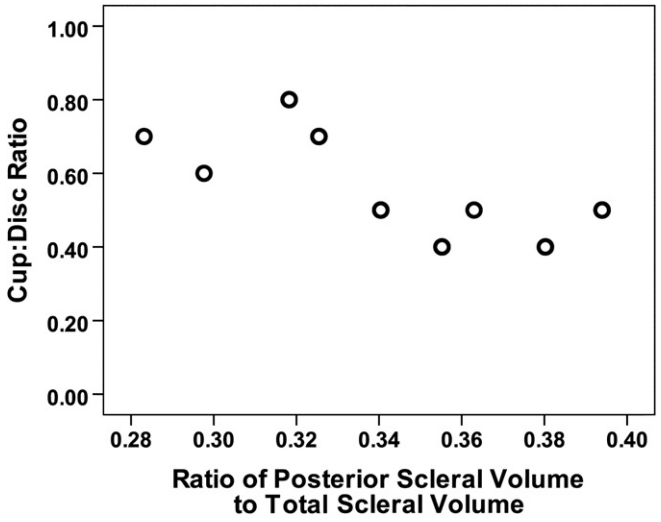

Fig. 7. Scatter plot of C:D ratio versus posterior scleral volume ratio.

et al. (1987) and Németh (1990) who found correlations between axial length and posterior coat thickness. Their studies were both limited by the use of ultrasound biomicroscopy, meaning they were unable to track scleral thickness alone. Olsen et al. found no correlation between axial length and scleral thickness, but did not detail the methods used to reach this conclusion. Oliveira et al. (2006) found a correlation between axial length of the eye and anterior scleral thickness near the scleral spur.

The source of the correlation between axial length and scleral thickness is unclear. Sclera could thin due to a Poisson effect, where pressure-induced expansion of the eye shell leads to a thinning of the wall. Pressure-induced radial compression of the sclera could also play a role, as the radial modulus of sclera has been found to be significantly lower than its circumferential modulus (meaning that it is easier to compress sclera radially than it is to stretch it longitudinally) (Battaglioli and Kamm, 1984). Arguing against this, our study found no significant differences between the axial lengths, mean scleral thicknesses, or posterior thicknesses of the low-and high-pressure groups, suggesting that purely mechanical stretching or compression of scleral tissue is unlikely to account for significant changes in thickness or axial length. The work of Lee et al. (2004) supports this conclusion, as they found that excised sclera only thinned significantly when pressurized to IOP levels of 60 mmHg or higher. Furthermore, from our preliminary data we propose that there is a relative change in scleral volume with axial length that is specific to the posterior region. If confirmed by a larger study, this phenomenon would be difficult to explain with a mechanical effect. Together these observations suggest that as the eye lengthens, there are active changes in the distribution of scleral tissue marked notably by a relative loss of tissue in the posterior region.

This is in agreement with research on the pathogenesis of myopia, a disease marked by axial elongation of the eye and scleral thinning at the posterior pole (Mitchell et al., 1999; Xu et al., 2007). There is growing evidence that these changes are the result of scleral remodelling. Interestingly, myopia is known to be related to glaucoma: myopes are at increased risk of developing the disease (Fong et al., 1990; Mitchell et al., 1999; Xu et al., 2007). The ostensibly glaucomatous eyes in this study were observed to be axially-elongated and had thinner posterior sclera relative to normal eyes and hence may have been myopic.

These traits may also be indicative of scleral changes in glaucoma, however, as there is evidence for scleral remodelling playing a role in the disease. Németh (1990) observed a strong multiple correlation between increasing IOP, axial lengthening of the eye and posterior coat thinning in adult glaucoma patients. Tane and Kohno (1986) found a significant thickening of the posterior choroid and sclera after surgical IOP reduction in adult glaucoma patients. Downs et al. (2001) observed significant posterior scleral thinning in monkey eyes with experimentally induced ocular hypertension. Jonas et al. observed that the lamina cribrosa thinned with axial length (Jonas and Holbach, 2005) and was thinner in glaucomatous than in normal eyes (Jonas et al., 2004). Furthermore, IOP-induced axial lengthening has been proposed in juvenile glaucoma (Fong et al., 1990), where afflicted eyes typically lengthen faster than can be accounted for by normal growth. Surgical reduction of IOP was observed to reduce elongation to normal rates (Kiefer et al., 2001; Law et al., 2001). It is possible that thinning at the posterior pole—whether induced by myopia, IOP, or other unidentified factors—reduces the mechanical strength of sclera in the vicinity of the ONH, leaving it weaker and exposed to IOP-induced glaucomatous damage.

A study by Ren et al. (2009) confirms elements of this hypothesis, finding that axially-elongated glaucomatous eyes did have thinner scleras than normal eyes of average length. They found, however, that glaucomatous eyes of normal length did not differ appreciably in scleral thickness. This study, however, dealt only with secondary angle closure glaucoma and had a large age gap between the axially-elongated (mean 27.9 years) and normal groups (mean 43.3 years), suggesting a possible role for age-associated differences in scleral stiffness in their findings (Friberg and Lace, 1988; Rada et al., 2000). We would note that it is not only scleral thickness that determines the biomechanics of the corneoscleral shell: biomechanics are also dependent on the material properties of the sclera (effective stiffness). Although extremely technically challenging, it would be very useful to see how stiffness and thickness co-vary in human eyes and how this relationship changes with age.

This study has several limitations. The small sample size limits its predictive ability. Also, in order to image the eyes, fixation was necessary. Post-mortem corneal swelling has been observed previously (Pels and Schuchard, 1983), so the corneal region was excluded from results. It is unknown whether fixation causes shrinkage or swelling in sclera (Olsen et al., 1998). Since scleral thickness is not dependent on active transport processes, however, there is little reason to believe that it will change post-mortem. Furthermore, if changes do occur, it is reasonable to assume similar behaviour across the eyes, so the results presented here likely present an accurate relative representation of live sclera.

The resolution of the MRI scans, while very high for that imaging modality, is still coarse on the scale of the microscopic tissues of the eye. Features below 80 μm in size would not be apparent in our images. This is of particular consequence when identifying anatomical boundaries during segmentation, as these boundaries underlie the results. Because this work presents results averaged over a region, however, it is less sensitive to the limitations of resolution than an approach using measurements at single points. Specifically, in the case of a single measurement, an error of one pixel during segmentation could result in a significant (up to 80 μm) discrepancy. However, it is likely in a given region that there are discrepancies favouring both thinner and thicker sclera, so that when thicknesses are averaged across the approximately 2500 measurements for a given region, this discrepancy would have little effect.

We were unable to obtain further details of the ostensibly glaucomatous eyes, other than to note the glaucomatous appearance of the ONH on HRT. The HRT imaging of post-mortem ONHs may be subject to artifact, in particular collapse of the central vessels, although this is unlikely to affect the area-based optic disc parameters used in this study. Special care was taken in the imaging procedure to help eliminate other limitations of post-mortem imaging. In order to allow a clear view of the optic disc, the vitreous and cornea (which is subject to post-mortem clouding) were both removed. Replacement optics were then used to allow direct imaging of the ONH. Fixation of the tissue meant that any post-mortem edema would be eliminated. The effect of the fixation process itself on the tissues of the optic disc is unclear, although it may result in some shrinkage. Previous studies (Jonas et al., 1992) have assumed a small, uniform effect across the optic disc, which is consistent with the unremarkable appearance of the optic discs relative to standard clinical images. Some difficulty was encountered when removing the vitreous. Although in most cases the vitreous separated cleanly from the fixed tissue, trace amounts remained adhered to the ONH surface in some eyes. In the case of two eyes, the adhered vitreous prevented direct viewing of the optic disc, meaning C:D ratios could not be calculated. Despite numerous attempts, we were unable to gain access to the IOP or medication history for any of the eyes, and thus have no information as to whether there is a correlation between the degree of ocular hypertension and any scleral parameters. The relationship observed between increasing C:D ratio and reduced posterior

scleral volume supports the idea that glaucomatous progression may result in changes in the sclera, however.

Some of the parameters discussed here are likely geometrically linked. Notably, scleral volume and thickness show similar correlations; these parameters were included for separate reasons in this analysis, however, justifying the inclusion of both. To our knowledge there is no reason to expect a geometric link between C:D ratio and scleral volume, suggesting a physiological basis for this observation.

In summary, we have measured the full scleral thickness distribution and other dimensions of the human eye. Significant variations were observed both intra-individually and inter-individually, supporting the hypothesis that ocular biomechanics may vary significantly between individuals. The fact that such dramatic variation was observed in a small study suggests that the variation in the population may be even greater. Further study of normal and glaucomatous eyes is necessary to characterize how scleral dimensions might affect the pathogenesis of this disease. Exploring the relationship between IOP, scleral thickness and volume, and axial elongation may be informative.

Acknowledgements

The authors thank the Eye Bank of Canada for providing donor tissue.

References

Battaglioli, J.L., Kamm, R.D., 1984. Measurements of the compressive properties of scleral tissue. Invest. Ophthalmol. Vis. Sci. 25, 59–65.

Burgoyne, C.F., Downs, J.C., Bellezza, A.J., Suh, J.K., Hart, R.T., 2005. The optic nerve head as a biomechanical structure: a new paradigm for understanding the role of IOP-related stress and strain in the pathophysiology of glaucomatous optic nerve head damage. Prog. Retin. Eye Res. 24, 39–73.

Downs, J.C., Ensor, M.E., Bellezza, A.J., Thompson, H.W., Hart, R.T., Burgoyne, C.F., 2001. Posterior scleral thickness in perfusion-fixed normal and early-glaucoma monkey eyes. Invest. Ophthalmol. Vis. Sci. 42, 3202–3208.

Fingeret, M., Medeiros, F.A., Susanna Jr., R., Weinreb, R.N., 2005. Five rules to evaluate the optic disc and retinal nerve fiber layer for glaucoma. Optometry 76, 661–668.

Fong, D.S., Epstein, D.L., Allingham, R.R., 1990. Glaucoma and myopia: are they related? Int. Ophthalmol. Clin. 30, 215–218.

Friberg, T.R., Lace, J.W., 1988. A comparison of the elastic properties of human choroid and sclera. Exp. Eye Res. 47, 429–436.

Guthoff, R., Berger, R.W., Draeger, J., 1987. Ultrasonographic measurement of the posterior coats of the eye and their relation to axial length. Graefes Arch. Clin. Exp. Ophthalmol. 225, 374–376.

Jonas, J.B., Berenshtein, E., Holbach, L., 2004. Lamina cribrosa thickness and spatial relationships between intraocular space and cerebrospinal fluid space in highly myopic eyes. Invest. Ophthalmol. Vis. Sci. 45, 2660–2665.

Jonas, J.B., Gusek, G.C., Guggenmoos-Holzmann, I., Naumann, G.O.H., 1988. Size of the optic nerve scleral canal and comparison with intravital determination of optic disc dimensions. Graefes Arch. Clin. Exp. Ophthalmol. 226, 213–215.

Jonas, J.B., Schmidt, A.M., Muller-Bergh, J.A., Schlotzer-Schrehardt, U.M., Naumann, G.O.H., 1992. Human optic nerve fiber count and optic disc size. Invest. Ophthalmol. Vis. Sci. 33, 2012–2018.

Jonas, J.B., Holbach, L., 2005. Central corneal thickness and thickness of the lamina cribrosa in human eyes. Invest. Ophthalmol. Vis. Sci. 46, 1275–1279.

Kiefer, G., Schwenn, O., Grehn, F., 2001. Correlation of postoperative axial length growth and intraocular pressure in congenital glaucoma–a retrospective study in trabeculotomy and goniotomy. Graefes Arch. Clin. Exp. Ophthalmol. 239, 893–899.

Lam, A., Sambursky, R.P., Maguire, J.I., 2005. Measurement of scleral thickness in uveal effusion syndrome. Am. J. Ophthalmol. 140, 329–331.

Law, S.K., Bui, D., Caprioli, J., 2001. Serial axial length measurements in congenital glaucoma. Am. J. Ophthalmol. 132, 926–928.

Lee, S., Geroski, D.H., Prausnitz, M.R., Edelhauser, H.F., 2004. Drug delivery through the sclera: effects of thickness, hydration, and sustained release systems. Exp. Eye Res. 78, 599–607.

Mitchell, P., Hourihan, F., Sandbach, J., Wang, J.J., 1999. The relationship between glaucoma and myopia: the Blue Mountains Eye Study. Ophthalmology 106, 2010–2015.

Németh, J., 1990. The posterior coats of the eye in glaucoma. An echobiometric study. Graefes Arch. Clin. Exp. Ophthalmol. 228, 33–35.

Norman R.E., 2008. Influence of the Scleral Shell on the Biomechanical Environment of the Human Optic Nerve Head. MASc Thesis, Department of Mechanical and Industrial Engineering, University of Toronto. 2008.

Oliveira, C., Tello, C., Liebmann, J., Ritch, R., 2006. Central corneal thickness is not related to anterior scleral thickness or axial length. J. Glaucoma 15, 190–194.

Olsen, T.W., Aaberg, S.Y., Geroski, D.H., Edelhauser, H.F., 1998. Human sclera: thickness and surface area. Am. J. Ophthalmol. 125, 237–241.

Pels, E., Schuchard, Y., 1983. Organ-culture preservation of human corneas. Doc. Ophthalmol. 56, 147–153.

Quigley, H.A., Flower, R.W., Addicks, E.M., McLeod, D.S., 1980. The mechanism of optic nerve damage in experimental acute intraocular pressure elevation. Invest. Ophthalmol. Vis. Sci. 19, 505–517.

Rada, J.A., Achen, V.R., Penugonda, S., Schmidt, R.W., Mount, B.A., 2000. Proteoglycan composition in the human sclera during growth and aging. Invest. Ophthalmol. Vis. Sci. 41, 1639–1648.

Ren, R., Wang, N., Li, B., Li, L., Gao, F., Xu, X., Jonas, J.B., 2009. Lamina cribrosa and peripapillary sclera histomorphometry in normal and advanced glaucomatous Chinese eyes with various axial length. Invest. Ophthalmol. Vis. Sci. 50, 2175–2184.

Rosner, B., 1982. Statistical methods in ophthalmology: an adjustment for the intraclass correlation between eyes. Biometrics 38, 105–114.

Sigal, I.A., Flanagan, J.G., Tertinegg, I., Ethier, C.R., 2004. Finite element modeling of optic nerve head biomechanics. Invest. Ophthalmol. Vis. Sci. 45, 4378–4387.

Sigal, I.A., Flanagan, J.G., Ethier, C.R., 2005. Factors influencing optic nerve head biomechanics. Invest. Ophthalmol. Vis. Sci. 46, 4189–4199.

Sigal, I.A., Flanagan, J.G., Tertinegg, I., Ethier, C.R., 2009a. Modeling individual-specific human optic nerve head biomechanics. Part I: IOP-induced deformations and influence of geometry. Biomech. Model. Mechanobiol. 8, 85–98.

Sigal, I.A., Flanagan, J.G., Tertinegg, I., Ethier, C.R., 2009b. Modeling individual-specific human optic nerve head biomechanics. Part II: influence of material properties. Biomech. Model. Mechanobiol. 8, 99–109.

Tane, S., Kohno, J., 1986. The microscopic biometry of the thickness of the human retina, choroid and sclera by ultrasound. Proc. XXVth Int. Congress Ophthalmol., 275–277.

Xu, L., Wang, Y., Wang, S., Wang, Y., Jonas, J.B., 2007. High myopia and glaucoma susceptibility the Beijing Eye Study. Ophthalmol. 114, 216–220.